Multicell Hybrid Switched Capacitor Boost Converter with High Voltage Conversion Ratio

Yenan Chen, Jaeil Baek and Minjie Chen
Department of Electrical Engineering
Andlinger Center for Energy and the Environment
Princeton University, Princeton, NJ, USA
Email: {yenanc, jaeil.baek, minjie}@princeton.edu

***Abstract*—This paper presents a family of merged-two-stage resonant-switched-capacitor boost converters with a *Linear Extendable Group Operated Boost* (LEGO-Boost) architecture. In the LEGO-Boost architecture, multiple resonant voltage doubler units are connected in parallel to interface with a high current input source; multiple switched-capacitor units are connected in series to interface with a high voltage output load. The operation of the resonant voltage doubler units and the switched-capacitor units are merged to create mutual advantages: the resonant voltage doubler units are used as current sources to soft-charge the series stacked switched-capacitor units and maintain voltage balancing; the stacked switched-capacitor units are used to multiply the voltage without charge sharing loss and switching loss (achieving soft-switching and soft-charging). All active switches in the LEGO-Boost architecture are configured as ground referenced half-bridge circuits. It offers advantages of high reliability, high scalability and low cost for applications such as grid-interface photovoltaic and fuel cell systems. The effectiveness of the LEGO-Boost architecture is verified by a 20 V-to-240 V 535 W (1:12 voltage conversion ratio) prototype with 94.2% peak efficiency and over 215 W/in^3 power density.**

***Index Terms*—switched-capacitor converter, resonant converter, soft-switching, soft-charging, photovoltaic, fuel cell.**

I. Introduction

One major challenge of interfacing photovoltaic (PV) and fuel cell energy systems with the electric grid is the large difference between the input voltage (usually 20 V–30 V) and the output voltage (usually a few hundred volts) [1]–[5]. High conversion ratio power converters are also needed in many other applications including LED drivers, CPU power supplies, and Uninterruptible Power Supplies (UPS) [6]–[10]. One popular approach of designing high voltage conversion ratio power converters is to use transformer or coupled inductor derived dc-dc converters [2]–[4], [6], [11]. High voltage conversion ratio can be easily achieved by adopting high winding turns-ratio. However, an isolated approach for non-isolated applications usually leads to large core volume and significant core loss [12]. The switching frequency of these systems are usually limited by the characteristics of magnetic materials.

Switched-capacitor (SC) circuits are becoming increasingly attractive due to their high efficiency at large voltage conversion ratio, very high power density, and magnetic-free implementation [13]. However, the voltage difference between two capacitors in the SC converters incurs large transient current and high charge-sharing loss when they are connected in parallel. The performance of a SC converter is also limited by the switching loss, which dominate the system loss when the SC circuit is operating at high frequencies. The switching loss of switched-capacitor circuits can be reduced by adopting the resonant-switched-capacitor approach [14], [15]. By employing resonance between capacitors and inductors, the current in the switched-capacitor circuit becomes sinusoidal and soft-switching can be achieved (both zero-current-switching and zero-voltage-switching). The charge-sharing loss can be reduced or fully eliminated by adopting the soft-charging mechanism - avoid connecting two capacitors in parallel by innovatively adding or reusing inductors. [9], [16] removed the dc-link capacitors between the SC stage and the buck stage and merged the two power conversion stages together. The buck inductors are reused to soft-charge the capacitors. The merged-two-stage approach extended the voltage conversion ratio, created the voltage regulation capability, and improved the efficiency and power density.

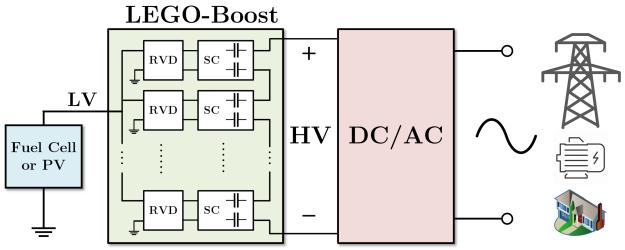

Fig. 1. Block diagram of the LEGO-Boost architecture with multiple Resonant Voltage Doubler (RVD) units and switched-capacitors (SC) units. This system can be linearly extended and group operated to cover a wide range of applications, e.g., photovoltaic and fuel cell energy systems.

This paper presents a merged-two-stage resonant-switched-capacitor boost converter with a *Linear Extendable Group Operated Boost* (LEGO-Boost) architecture. As illustrated in Fig. 1, the LEGO-Boost architecture comprises a few resonant voltage doubler (RVD) units and a few switched-capacitor (SC) units. The RVD units interface with input sources (e.g. PV cells, fuel cells) and double the input voltage. The RVD units also function as current sources to feed energy into the series-stacked SC units, which linearly boost the output voltage. This paper introduces the operation principles of the LEGO-Boost architecture, and develops design methods and control strategies to achieve zero-current-switching (ZCS) and soft-charging. With merged-two-stage operation of the RVD units and the SC units, the decoupling capacitors are

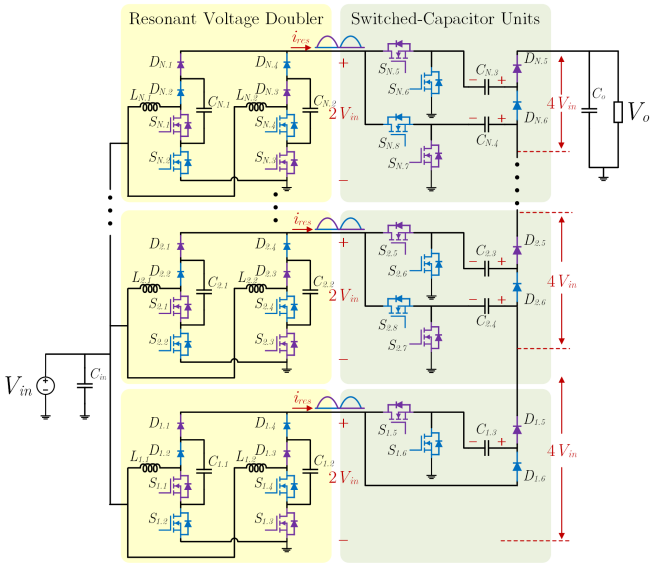

Fig. 2. The LEGO-Boost converter with N parallel-input series-output modules, each comprising a resonant voltage doubler on the input side and a capacitive-isolated voltage multiplier on the output side. There is no decoupling capacitor between the two stages. The intermediate bus is not a voltage source but a current source which enables soft-charging of the capacitors and soft-switching of the switches in the switched-capacitor stage.

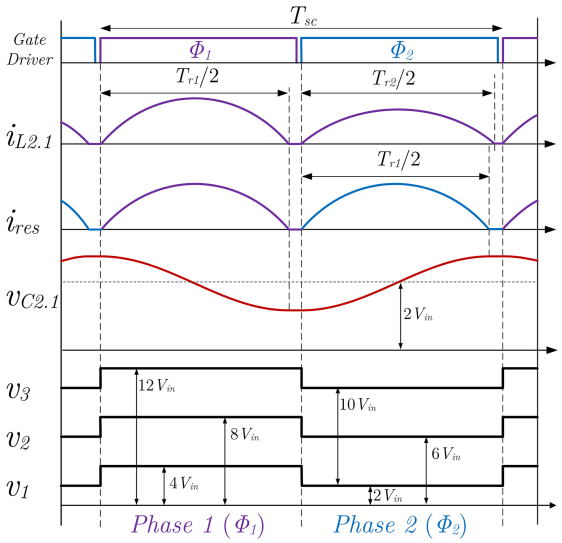

Fig. 3. Gate driver signals and key operating waveforms of a LEGO-Boost converter with three parallel-input series-output submodules (Fig. 2).

eliminated and ZCS is achieved in all switches. The parallel-input series-output configuration natually guarantees voltage balancing of the SC units and current sharing of the RVD units. The LEGO-Boost converter is highly modular and can be linearly extended both in series and in parallel to cover a wide operation range. The effectiveness of the LEGO-Boost architecture is verified by a 20 V-to-240 V 500 W (1:12 boost ratio) prototype with 94.2% peak efficiency and over over 215 W/in^3 power density.

The remainder of this paper is organized as follows: Section II introduces the circuit topology of the LEGO-Boost architecture and its operation principles to achieve ZCS of switches and soft-charging of capacitors. Section III explains the advantages of the LEGO-Boost architecture. Section IV presents the design of a high performance LEGO-Boost converter. The experimental results are summarized in Section V. Finally, Section VI concludes this paper.

II. Principles of the LEOG-Boost Architecture

Fig. 2 shows one example topology with the LEGO-Boost architecture. The topology can be interpreted as an array of parallel-input series-output modules. Each module contains a resonant voltage doubler with two interleaved phases and a SC unit. The SC units are connected in series as capacitive-isolated voltage multiplier circuits. Both the resonant voltage doubler and the SC unit operates with a complementary 50% duty ratio. The voltage conversion ratio is $1:2$ for both the resonant voltage doubler and the SC unit. Thus, the voltage conversion ratio of one module is $1:4$ and the overall voltage conversion ratio from the input to the output is $1:4N$ where N is the number of the parallel-input series-output modules.

Unlike a traditional two-stage dc-dc architecture with an intermediate bus and a decoupling capacitor, the LEGO-Boost converter eliminates the decoupling capacitors and merges the resonant voltage doubler stage and SC stage to enable soft-charging and soft-switching. Fig. 3 shows the gate driver signals and key waveforms of the merged-two-stage operation of the LEGO-Boost converter with three parellel-input series-output modules and a voltage conversion ratio of $1:12$. All the switches are controlled by two complementary gate driver signals with 50% duty ratio (Φ_1 and Φ_2). Φ_1 turns on all the switches named by odd number ($S_{X.1}, S_{X.3}, \cdots$) in Phase 1 and Φ_2 turns on all the switches named by even number ($S_{X.2}, S_{X.4}, \cdots$) in Phase 2. Fig. 4 presents the operating status of the LEGO-Boost converter in Phase 1 and Phase 2.

Phase 1 – Φ_1 is high and Φ_2 is low. The resonant current between the inductors and capacitors begins from zero, which enables soft-charging of all the switched capacitors and also creates zero-current turn-on opportunities for all switches. Take $L_{2.1}$ as an example: $L_{2.1}$ is connected in series with $C_{2.1}$, $C_{2.3}$ and $C_{3.4}$ during Phase 1. $C_{2.1}$ and $C_{2.3}$ are discharged while $C_{3.4}$ is charged by the resonant current. Assuming all inductors have identical inductance L_r, all capacitors in the resonant voltage doubler stage have identical capacitance C_r, and all capacitors in the SC stage have identical capacitance C_s. The resonant period is:

$$T_{r1} = 2\pi\sqrt{L_r \frac{C_r}{1+2C_r/C_s}}. \tag{1}$$

Once the resonant current falls back to zero after a half cycle, the resonance as well as the charging/discharging are terminated. The peroid of Phase 1 must be longer than half resonant cycle to guarantee zero-current turn-off of all diodes.

Phase 2 – the soft-charging and soft-switching mechanism in Phase 2 is similar to Phase 1. The resonance still begins with zero current. In Phase 2 $L_{2.1}$ is only in series with $C_{2.1}$. $C_{2.1}$ is charged by $i_{L2.1}$ while $C_{2.3}$ is charged by $i_{L2.2}$, and

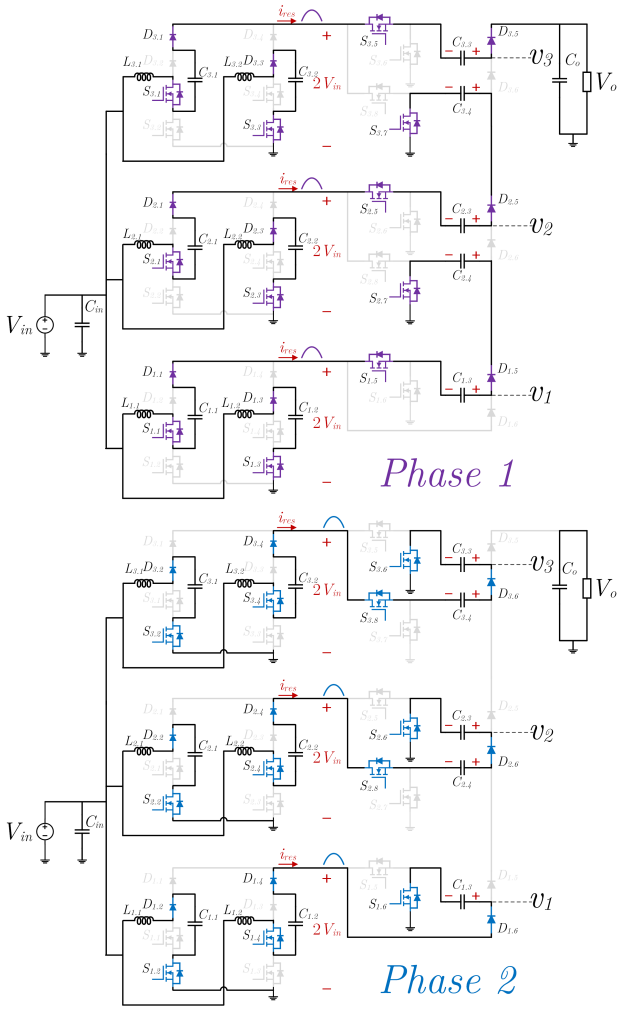

Fig. 4. Two operating phases of the LEGO-Boost converter. In both phases all capacitors are soft-charged by the inductors of the resonant voltage doublers. The capacitors of the switched-capacitor stage can be sized small benefiting from the eliminated charge sharing loss.

$C_{3.4}$ is discharged by $i_{L3.2}$. The resonant period of $L_{2.1}$ – $C_{2.1}$ in Phase 2 is:

$$T_{r2} = 2\pi\sqrt{L_r C_r}. \tag{2}$$

The period of Phase 2 also should be longer than half cycle of T_{r2} to achieve zero current switching.

Notice that the resonant elements, the resonant period and the current amplitude for one resonant inductor in two operating phases are different. For resonant inductor $L_{2.1}$, the current amplitude is larger and the resonant cycle is shorter in Phase 1. Furthermore, there are two special cases: $L_{3.1}$ is connected in series with $C_{3.1}$, $C_{3.3}$ and the output filter capacitor C_o during Phase 1; $L_{1.2}$ is connected in series with $C_{1.2}$ and $C_{1.3}$ during Phase 2. The different resonant paths result in two additional resonant periods:

$$T_{r3} = 2\pi\sqrt{L_r \frac{C_r}{1 + C_r/C_s + C_r/C_o}}. \tag{3}$$

$$T_{r4} = 2\pi\sqrt{L_r \frac{C_r}{1 + C_r/C_s}}. \tag{4}$$

Obviously T_{r2} is the longest resonant period and the switching period T_{sc} must be longer than T_{r2} to guarantee soft-switching and soft-charging. Another consideration for the resonant cycles is that the difference among them should be minimized. Otherwise the long zero-current status before the next operating phase reduces the utilization of the switches and increases the power stress for the same average power delivered. Therefore C_s and C_o should be much larger than C_r to constrain all the resonant cycles within a narrow range.

III. Advantages of LEGO-Boost Architecture

A. Soft-Charging and Soft-Switching

The merged-two-stage operation brings the advantages of soft-charging for all capacitors, and eliminates the charge-sharing loss. The resonant operation enables the ZCS for all switches and higher switching frequency with smaller passive components. The switching loss from the parasitic capacitance (C_{oss}) of semiconductor devices still exists and is proportional to the switching frequency. Wide band gap devices (GaN and SiC) with smaller parasitic capacitance are preferable for the LEGO-Boost converter. The intermediate buses in the three modules in Fig. 4 are not tied together even if they have equal bus voltage. This configuration guarantees every switched capacitor in the LEGO-Boost converter is charged/discharged by the same resonant current in both operation phases, which enables current sharing in the resonant voltage doublers.

B. Low Voltage and Current Stress for Semiconductor Devices

The parallel-input series-output configuration of LEGO-Boost architecture can reduce the switching stress for semiconductors by decoupling the voltage stress and current stress. In a traditional boost converter, both of the switch and diode need to block the maximum output voltage and carry the peak input current. The total die area of the semiconductor devices will be much higher than the normal operation power. In the LEGO-Boost architecture, the switches and diodes in the resonant voltage doubler stage only need to block the low input voltage V_{in}; the voltage stress of the switches in SC stage is $2V_{in}$ and the voltage stress of the diodes in SC stage is $4V_{in}$ ($2V_{in}$ for the top diode $D_{N.5}$). The voltage stress of the semiconductor devices is not related to the overall output voltage. As illustrated in Fig. 4, all the switches and diodes carry the same resonant current which is only a small fraction of the total input current. In order to simplify the analysis, C_s and C_o are assumed with infinite capacitance and the switching frequency f_{sc} is equal to all the resonant frequencies. For the LEGO-Boost converter with N parallel-input series-output modules (the voltage conversion ratio is 1:4N), the total input power is $P_{in} = V_{in}I_{in}$ and the peak current of each resonant inductor is:

$$I_{pk} = \frac{\pi I_{in}}{4N}. \tag{5}$$

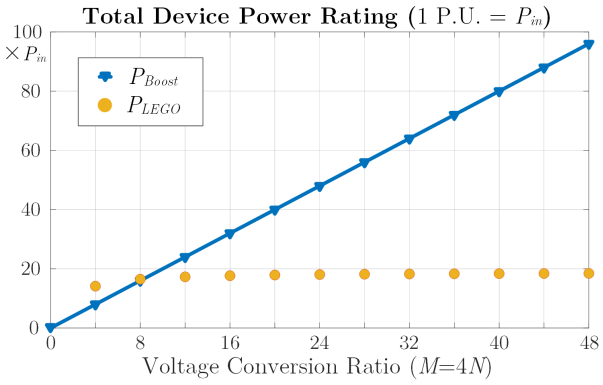

Fig. 5. Comparison of the total switch power rating between a LEGO-Boost converter and a traditional boost converter with identical input power, input voltage and voltage conversion ratio.

I_{pk} is assumed to be the current stress for all switches. The total power rating of the semiconductor devices of the N resonant voltage doubler units is:

$$P_{RVD} = 8NV_{in}I_{pk} = 2\pi P_{in}. \tag{6}$$

The voltage ripple in the resonant capacitor is neglected. The total power rating of the switches in the N SC units is:

$$\begin{aligned} P_{SC} &= (4N-2+1)\times 2V_{in}I_{pk} + (2N-1)\times 4V_{in}I_{pk} \\ &= (16N-6)V_{in}I_{pk} = (4-\frac{3}{2N})\pi P_{in}. \end{aligned} \tag{7}$$

The total power rating of the LEGO-Boost converter as a function of the voltage conversion ratio $M = 4N$ is:

$$P_{LEGO} = (6-\frac{6}{M})\pi P_{in}. \tag{8}$$

For a boost converter with the same operation range, assuming constant current in the boost inductor, the total power rating of the semiconductor devices is:

$$P_{Boost} = 2MP_{in}, \tag{9}$$

where M=4N is the voltage conversion ratio. Fig. 5 compares the total power rating of the semiconductor devices in the LEGO-Boost converter and a traditional boost converter as a function of the voltage conversion ratio. The switch rating of a traditional boost converter increases linearly with the voltage conversion ratio become extremely high with high voltage conversion ratio. The total device power rating of LEGO-Boost converter has a upper limit which equals to $6\pi P_{in}$, and is independent of the voltage conversion ratio when N is high. Moreover, the passive components (inductors and capacitors) of the LEGO-Boost architecture scales well with high frequency. It also leverages the high power density of capacitors and has significantly reduced inductor size. The LEGO-Boost architecture fits particularly well to applications where high voltage conversion ratio is needed.

C. Modular, Scalable and Reliable

The LEGO-Boost architecture is highly modular and linearly scalable. The system power rating and voltage conversion ratio can be easily extended by replicating the same parallel-input-series-output modules. Note the isolation capacitors (e.g., $C_{1,3}$, $C_{2,3}$, $C_{2,4}$) need to be selected accordingly. As an example, the dc blocking voltage of the five capacitors in the SC stages ($C_{1.3}$ – $C_{3.3}$, from bottom to top) is $2V_{in}$, $4V_{in}$, $6V_{in}$, $8V_{in}$, $10V_{in}$ respectively. As a capacitive-isolated topology, the high voltage stress is transferred from semiconductor devices to capacitors, which enables the utilization of low voltage rating devices with high performance (e.g., DrMOS). The voltage stress of the semiconductor devices remains the same regardless of the output voltage level (it is only related to the input voltage V_{in}). The current stress is only related to the total output power. As the voltage conversion increase, the efficiency of a LEGO-Boost converter doesn't drop but remains the same. While in most dc-dc converter designs, the efficiency drops as the voltage conversion ratio increases.

All active switches in the LEGO-Boost architecture can be implemented as ground-referenced half-bridge circuits with diode voltage multipliers. The gate drive circuits are straight-forward to implement with commercial half-bridge gate drivers. No level-shifting is needed. The system can achieve very high modularity, scalability, and reliability.

IV. Example LEGO-Boost Converter Design

An example design of a 20 V-240 V, 535 W LEGO-Boost converter targeting PV and fuel cell applications is presented in this paper. The voltage conversion ratio is 1:12 and three parallel-input series-output modules are used in this design. The circuit topology is same as the one shown in Fig. 4.

The switching frequency is chosen as 450 kHz. The inductance of all the resonant inductors is 220 nH, the value of C_r, C_s and C_o is 0.4 μF, 6 μF and 6 μF, respectively. The four resonant period are $T_{r1} = T_{r3} = 1751$ns, $T_{r2} = 1864$ns, $T_{r4} = 1805$ns. All resonant periods are smaller than the switching period. A margin of 180 ns is set to guarantee ZCS and soft-charging in each half switching cycle. The current waveform of the resonant inductors and the voltage waveform of resonant capacitors can be obtained from the $L-C$ resonant equations in each operating phase and is shown in Fig. 6. Due to different resonant cycles, the current amplitudes of the six resonant inductors are also slightly different. The amplitude of the resonant current is related to the resonant cycle:

$$I_{pki} = \frac{\pi I_{in}}{4N}\frac{T_{sc}}{T_{ri}}, i = \{1,2,3,4\}. \tag{10}$$

In this case the maximum peak resonant current is $I_{pk1} = I_{pk3} = 8.9$ A, which is 130% of the ideal case. The voltage ripples of both $C_{1.1}$ and $C_{1.2}$ are closed to $\pm$6.2V. The voltage ripple of capacitors in the SC stages is much smaller due to the high capacitance. Larger capacitance in the SC stage can also reduce the differences between resonant cycles and reduce the current amplitudes.

All half-bridge circuits are implemented as GaN-based LMG5200 from Texas Instruments. Two 80 V/10 A GaN switches and the half-bridge gate driver are integrated into one 6 mm$\times$8 mm chip. The parameters of other components and the equivalent capacitance considering capacitance degradation at high voltage are listed in Table I.

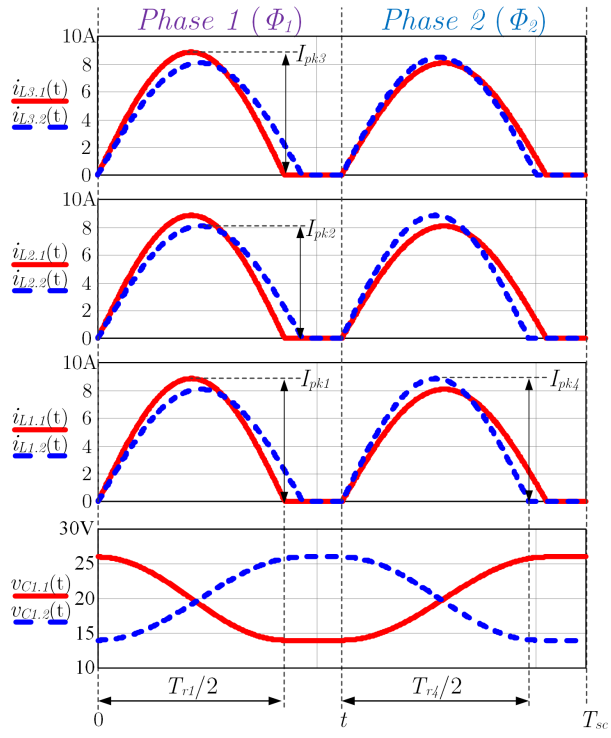

Fig. 6. Analytical current waveforms of all six resonant inductors and voltage waveforms of capacitors $C_{1.1}$ and $C_{1.2}$. The resonant cycle and current amplitude are slightly different due to the different resonant elements. The voltage ripple is ±6.2V.

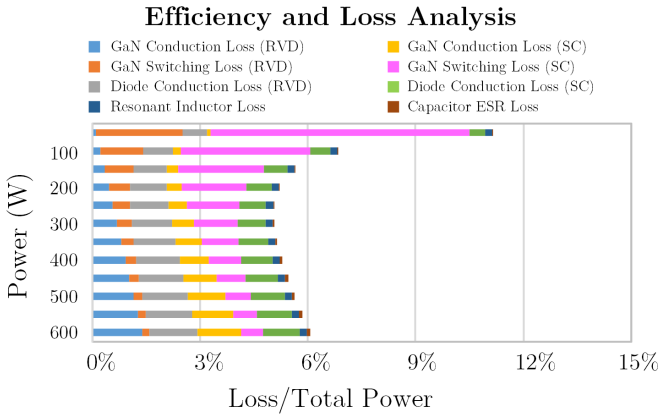

Fig. 7. Calculated power loss of the Resonant Voltage Double (RVD) stage and the Switched-Capacitor (SC) stage. The peak efficiency is estimated as 95.4% at half load (267 W).

Fig. 7 performs a detailed loss analysis for the LEGO-Boost converter. The power loss can be mainly divided into: GaN switch conduction loss and switching loss, diode conduction loss, inductor loss, and ESR loss of capacitors. The switching loss (C_{oss} loss) of the GaN switches (especially in the SC stage) dominates the total power loss at light load since it is only related to the operating voltage and frequency. One way to mitigate this problem is to reduce the switching frequency at light load. However, this approach will increase the peak resonant current as well as the conduction loss since

TABLE I
PARAMETERS OF THE 20V-240V/500W LEGO-BOOST PROTOTYPE

$S_{X.1} - S_{X.6}$	LMG5200, 80V/10A/15mΩ
$D_{X.1} - D_{X.4}$	MBR2045MFS, 45V/20A
$D_{X.5} - D_{X.6}$	FERD40H100S, 100V/40A
$L_{1.1} - L_{3.2}$	FP0705R1-R22, 220nH
$C_{X.1} - C_{X.2}$	100nF×4, C_{eq} = 400nF, 50V, C0G, TDK
$C_{1.3}$	2.2μF×8, C_{eq} = 7.86μF, 100V, X7S, TDK
$C_{2.4}$	4.7μF×8, C_{eq} = 6.64μF, 100V, X7S, TDK
$C_{2.3}$	2.2μF×6, C_{eq} = 6.6μF, 250V, X7T, TDK
$C_{3.4}$	2.2μF×8, C_{eq} = 7.2μF, 250V, X7T, TDK
$C_{3.3}$	2.2μF×10, C_{eq} = 7.67μF, 250V, X7T, TDK
C_o	2.2μF×12, C_{eq} = 7.7μF, 250V, X7T, TDK
C_{in}	10μF×12, 50V, X5R, Murata
Switching Frequency	450kHz

the resonant frequency remains the same. Thus, there is an optimal switching frequency which balances the switching loss and conduction loss, and also retains the peak current within the safety operation area of the semiconductor devices. The optimal frequency for efficiency operation can be found experimentally and will be presented in the next section.

Since the switching loss of the GaN switches in the SC stage is almost four times of the switching loss of the RVD stage, the converter efficiency can be significantly improved by reducing the switching frequency of the SC stage. Fig. 8 illustrates the principles of dual-frequency operation concept for the LEGO-Boost architecture, where the RVD stage operates at twice frequency of the SC stage. The switches in the voltage doubler stage are still controlled by the same gate driver signals Φ_1 and Φ_2 with switching frequency of f_{sc}. The switches in the switched-capacitor stage are controlled by Φ_A and Φ_B with lower switching frequency ($\frac{1}{2}$ of f_{sc} in this example case). A current balancing mechanism is needed to ensure current sharing between the two resonant voltage doubler circuit. One way to balance the power is to implement the two seperate inductors as a coupled inductor with carefully selected common-mode and differential-mode inductance.

Furthermore, Synchronized Rectification (SR) can be utilized to reduce the forward voltage drop loss of diodes. Fig. 9 shows the circuit topology of a SR resonant voltage doubler. The SR switches can utilize the same low voltage device as the low side switches. The SR gate driver signals need to be modified from the original gate driver signals (Φ_1 and Φ_2) to guarantee zero-voltage switching (ZVS) for the SR switches. The overall efficiency can be improved by about 0.5% with the SR resonant voltage doubler. Synchronized rectification also can be applied to the switched-capacitor stage. However, a SR rectification implementation requires additional isolated gate drivers with isolated power supply, which increases the cost and the system complexity.

V. EXPERIMENTAL RESULTS

A 20 V-240 V, 535 W prototype with the same parameters as listed in Table I is built and tested. The prototype is shown in Fig. 10 and the PCB layout is given in Fig. 11. All

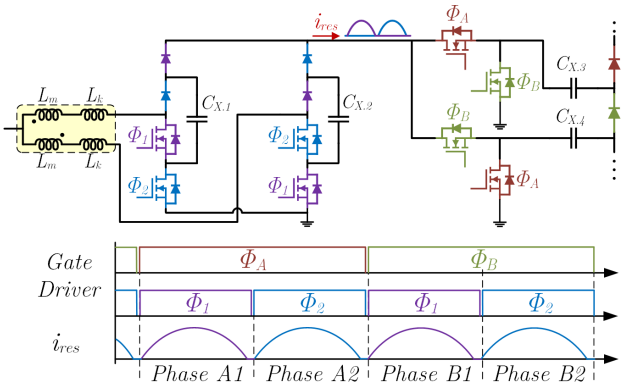

Fig. 8. A LEGO-Boost module with coupled inductor and the gate driver signals in dual-frequency operation: the switching frequency of the switched-capacitor stage is one half of the switching frequency of the resonant voltage doubler stage.

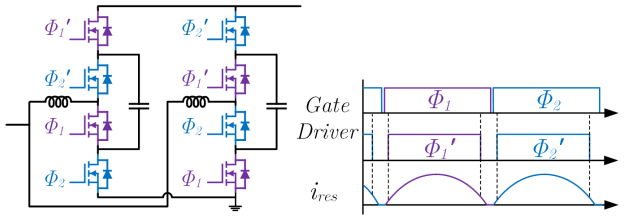

Fig. 9. Circuit schematic of the resonant voltage doubler with Synchronized Rectification (SR) and the gate driver signals of the SR switches.

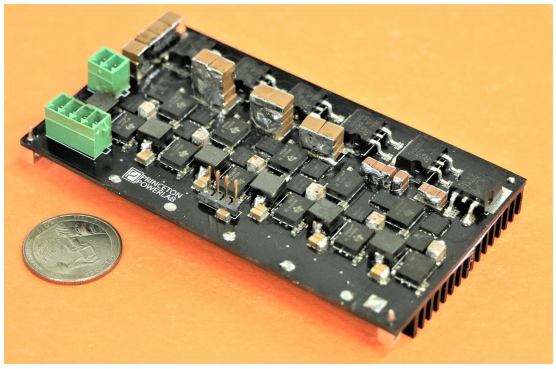

Fig. 10. Picture of the 20 V-240 V/535 W LEGO-Boost converter and a US quarter. One full piece of 100 mm×50 mm×10 mm heatsink is attached to the bottom side of the PCB.

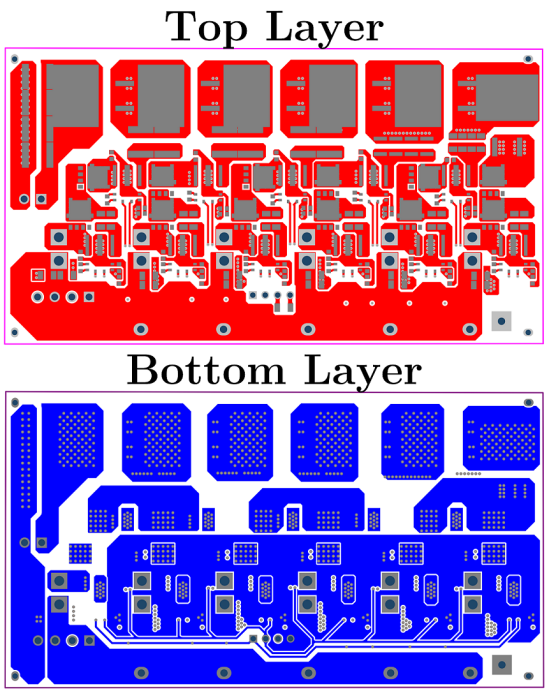

Fig. 11. PCB layout of the 20 V-240 V/535 W LEGO-Boost converter. The PCB size is 110 mm×60 mm and is highly modular. All components are placed on one side of the PCB.

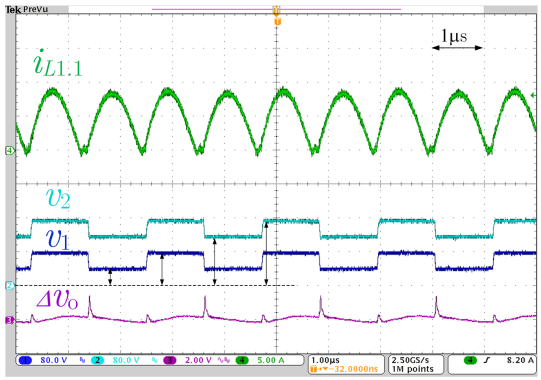

Fig. 12. Measured waveforms of the resonant current $i_{L1.1}$, two switch node voltages v_1 and v_2 of the SC stage, and the output voltage ripple. P_o = 535 W, f_{sc} = 450 kHz. v_1 and v_2 are labeled in Fig. 4.

components are placed on the top layer. The power density is 216 W/in^3 without heatsink. A 100mm×50mm×10mm heatsink is attached to the bottom side of the PCB. Fig. 12 shows the current of resonant inductor $L_{1.1}$, the switch node voltage in the switched-capacitor stage v_1 and v_2, and the output voltage ripple Δv_o with output power of 535 W. The switching frequency is 450 kHz. The resonant period is slightly shorter than the switching period. The amplitude of the resonant current is 9 A, which matches the theoretical calculation. The switch node voltage has a step of 40 V ($2V_{in}$) and the output voltage ripple is below 1.6 V (0.67% of V_o).

Fig. 13 shows the measured waveforms of two resonant inductors and two resonant capacitors in the same voltage doubler unit. The two current waveforms are different in Phase 1. The resonant cycle of $i_{L1.1}$ is T_{r1} (the shortest one) and the resonant cycle of $i_{L1.2}$ is T_{r2} (the longest one). In Phase 2 the resonant cycle of $i_{L1.1}$ is T_{r2} and the resonant cycle of $i_{L1.2}$ is T_{r4} ($T_{r1} < T_{r4} < T_{r2}$). Two resonant capacitors are charged/discharged in each operating phase and the voltage ripple is ±7 V with full power at 450 kHz.

Fig. 14 shows the drain-to-source voltage of switches $S_{1.2}$ and $S_{1.6}$. Due to the voltage ripple of resonant capacitor $C_{1.1}$, the voltage stress of $S_{1.2}$ is higher than the input voltage. While the voltage stress of $S_{1.6}$ still equals to $2V_{in}$ because $C_{1.3}$ is 15 times larger than $C_{1.1}$ and its voltage ripple is much smaller. The waveforms of resonant current and drain-source voltage verified the zero-current-switching operation.

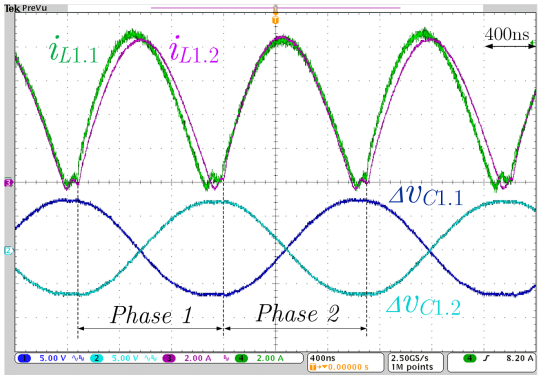

Fig. 13. Measured waveforms of the resonant current $i_{L1.1}$, $i_{L1.2}$ and voltage ripple of resonant capacitor $\Delta v_{C1.1}$, $\Delta v_{C1.2}$. P_o = 535 W, f_{sc} = 450 kHz. The amplitude and cycle of the resonant currents are slightly different.

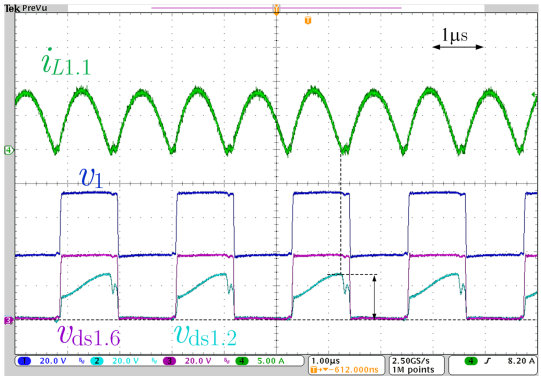

Fig. 14. Measured waveforms of the resonant current $i_{L1.1}$, switch node voltages v_1, drain-source voltage $v_{ds1.6}$, $v_{ds1.2}$. P_o = 535 W, f_{sc} = 450 kHz. The voltage stress of switches in the RVD units is higher than $2V_{in}$

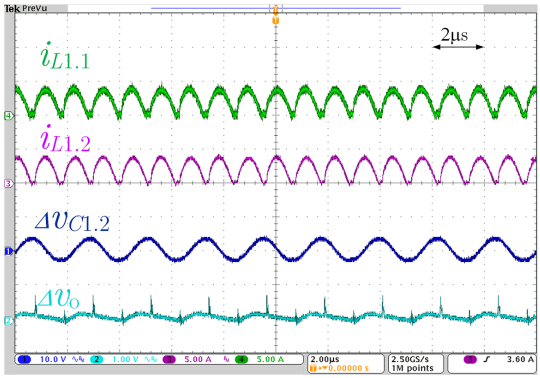

Fig. 15. Measured waveforms of the resonant current $i_{L1.1}$, $i_{L1.2}$, voltage ripple of resonant capacitor $\Delta v_{C1.2}$, and output voltage ripple Δv_o. P_o = 250 W, f_{sc} = 450 kHz.

Fig. 16. Measured waveforms of the resonant current $i_{L1.1}$, $i_{L1.2}$, voltage ripple of resonant capacitor $\Delta v_{C1.2}$, and output voltage ripple Δv_o. P_o = 250 W, f_{sc} = 200 kHz.

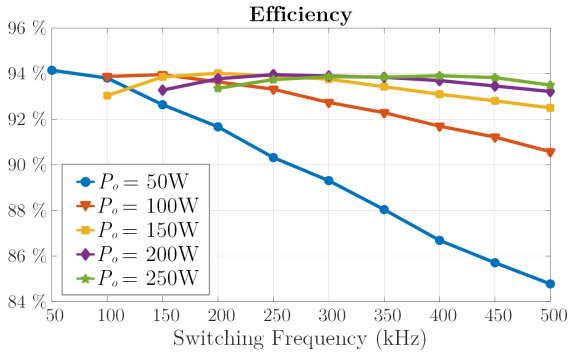

Fig. 17. Measured efficiency with P_o = 50 W, 100 W, 150 W, 200 W, 250 W and f_{sc} = 50 kHz, 100 kHz, 150 kHz, 200 kHz, 250 kHz, 300 kHz, 350 kHz, 400 kHz, 450 kHz, 500 kHz.

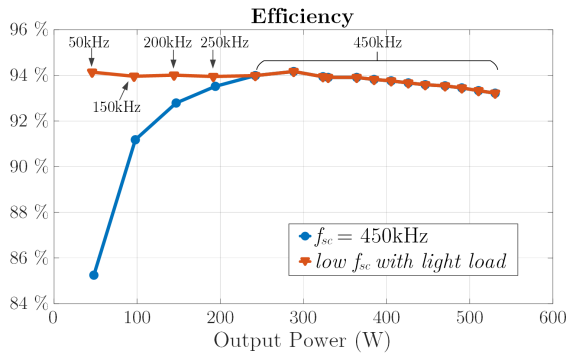

Fig. 18. Measured efficiency of the 20 V-240 V/535 W LEGO-Boost converter. Reducing the switching frequency can significantly improve the light load efficiency of the system.

Fig. 15 and Fig. 16 show the operating waveforms with output power of 250 W and two different switching frequencies (450 kHz and 200 kHz). With lower switching frequency the resonant current amplitude and resonant voltage ripple are higher since the resonant frequencies and output power remain the same. The output voltage ripple is also higher but still within 0.5% of the total output voltage. Lower switching frequency can reduce the switching loss but may increase the current stress as well as the conduction loss of the switches (the conduction ratio of device in each switching cycle is reduced with lower switching frequency but the conduction loss is related to the square of current, thus the overall conduction loss still increases).

To identify the optimal switching frequency for the LEGO-Boost converter at light load, the system efficiency is measured with multiple switching frequencies and the test results are compared in Fig. 17. At very low power level (50 W) the efficiency is improved from 84.8% to 94.2% by reducing the

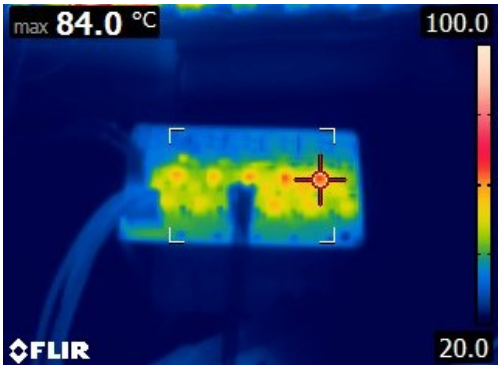

Fig. 19. Measured thermal image of the 20 V–240 V/535 W LEGO-Boost converter with a heat sink and without air cooling, P_o = 535 W, f_{sc} = 450 kHz. The hottest components are the GaN switches in the SC stages.

switching frequency from 500 kHz to 50 kHz. An "optimal" switching frequency can be identified according to the measurement results considering both the conduction loss and switching loss. The efficiency of the 20 V-240 V/535 W LEGO-Boost converter in the full power range is shown in Fig. 18. The efficiency at light load with a fixed switching frequency of 450 kHz rapidly drops due to the switching loss. Adaptive frequency control is applied to the LEGO-Boost converter to improve the light load efficiency (>94% from 50 W to 300 W). The peak efficiency is 94.2% with 300 W power. The full load efficiency is 93.2%. The thermal image of the LEGO-Boost converter with an output power of 535 W is shown in Fig. 19. The thermal image is captured with the 100 mm×25 mm×10 mm heatsink and without cooling fan. The hottest components are the GaN switches in the SC stages and the temperature of all the other components is below 60°C.

VI. Conclusions

This paper presents a LEGO-Boost architecture for high-ratio voltage conversion applications. The LEGO-Boost architecture is a merged-two-stage architecture: the resonant voltage doubler stage and the switched-capacitor stage are merged together to create mutual advantages. The operation principles of the LEGO-Boost converter are introduced, together with the switching strategies to achieve soft-charging and soft-switching. The LEGO-Boost architecture offers reduced switch stress, improved efficiency and power density, automatic voltage/current balancing, and very high modularity. We performed detailed loss analysis and two different methods are introduced to improve the efficiency. The effectiveness of the LEGO-Boost architecture is verified by a 20 V-240 V, 535 W prototype with peak efficiency of 94.2% and power density of 216 W/in^3 for photovoltaic and fuel cell applications.

Acknowledgment

The authors would like to thank the National Science Foundation (under Award #1847365) and Princeton E-ffiliates Program for supporting this work.

References

[1] F. Blaabjerg, Zhe Chen and S. B. Kjaer, "Power electronics as efficient interface in dispersed power generation systems," *IEEE Transactions on Power Electronics*, vol. 19, no. 5, pp. 1184-1194, Sept. 2004.

[2] M. Forouzesh, Y. Shen, K. Yari, Y. P. Siwakoti and F. Blaabjerg,"High-Efficiency High Step-Up DC–DC Converter With Dual Coupled Inductors for Grid-Connected Photovoltaic Systems," *IEEE Transactions on Power Electronics*, vol. 33, no. 7, pp. 5967-5982, July 2018.

[3] J. Wang, F. Z. Peng, J. Anderson, A. Joseph and R. Buffenbarger, "Low cost fuel cell converter system for residential power generation," *IEEE Transactions on Power Electronics*, vol. 19, no. 5, pp. 1315-1322, Sept. 2004.

[4] X. Zhao, C. Chen and J. Lai, "A High-Efficiency Active-Boost-Rectifier-Based Converter With a Novel Double-Pulse Duty Cycle Modulation for PV to DC Microgrid Applications," in *IEEE Transactions on Power Electronics*, vol. 34, no. 8, pp. 7462-7473, Aug. 2019.

[5] Y. Zhang et al., "Wide Input-Voltage Range Boost Three-Level DC–DC Converter With Quasi-Z Source for Fuel Cell Vehicles," in *IEEE Transactions on Power Electronics*, vol. 32, no. 9, pp. 6728-6738, Sept. 2017.

[6] Q. Zhao and F. C. Lee,"High-efficiency, high step-up DC-DC converters," in *IEEE Transactions on Power Electronics*, vol. 18, no. 1, pp. 65-73, Jan. 2003.

[7] M. Ahmed, C. Fei, F. C. Lee and Q. Li, "High-efficiency high-power-density 48/1V sigma converter voltage regulator module," *2017 IEEE Applied Power Electronics Conference and Exposition (APEC)*, Tampa, FL, 2017, pp. 2207-2212.

[8] S. Jiang, S. Saggini, C. Nan, X. Li, C. Chung and M. Yazdani, "Switched Tank Converters," in *IEEE Transactions on Power Electronics*, vol. 34, no. 6, pp. 5048-5062, June 2019.

[9] J. Baek, P. Wang, S. Jiang, M. Chen, "LEGO-PoL: A 93.1% 54V-1.5V 300A Merged-Two-Stage Hybrid Converter with a Linear Extendable Group Operated Point-of-Load (LEGO-PoL) Architecture," *IEEE 20th Workshop on Control and Modeling for Power Electronics (COMPEL)*, Toronto, 2019, pp. 1-8.

[10] R. Das and H. Le, "A Regulated 48V-to-1V/100A 90.9%-Efficient Hybrid Converter for POL Applications in Data Centers and Telecommunication Systems," *2019 IEEE Applied Power Electronics Conference and Exposition (APEC)*, Anaheim, CA, USA, 2019, pp. 1997-2001.

[11] W. Li, Y. Zhao, Y. Deng and X. He,"Interleaved Converter with Voltage Multiplier Cell for High Step-Up and High-Efficiency Conversion," in *IEEE Transactions on Power Electronics*, vol. 25, no. 9, pp. 2397-2408, Sept. 2010.

[12] H. Liu, H. Hu, H. Wu, Y. Xing and I. Batarseh, "Overview of High-Step-Up Coupled-Inductor Boost Converters," in *IEEE Journal of Emerging and Selected Topics in Power Electronics*, vol. 4, no. 2, pp. 689-704, June 2016.

[13] M. D. Seeman and S. R. Sanders, "Analysis and Optimization of Switched-Capacitor DC–DC Converters," in *IEEE Transactions on Power Electronics*, vol. 23, no. 2, pp. 841-851, March 2008.

[14] Y. Lei and R. C. N. Pilawa-Podgurski, "A General Method for Analyzing Resonant and Soft-Charging Operation of Switched-Capacitor Converters," in *IEEE Transactions on Power Electronics*, vol. 30, no. 10, pp. 5650-5664, Oct. 2015.

[15] D. Cao and F. Z. Peng, "A family of zero current switching switched-capacitor dc-dc converters," *2010 Twenty-Fifth Annual IEEE Applied Power Electronics Conference and Exposition (APEC)*, Palm Springs, CA, 2010, pp. 1365-1372.

[16] R. C. N. Pilawa-Podgurski, D. M. Giuliano and D. J. Perreault, "Merged two-stage power converter architecture with soft-charging switched-capacitor energy transfer," *2008 IEEE Power Electronics Specialists Conference*, Rhodes, 2008, pp. 4008-4015.